SUPPORTING INFORMATION

Supporting Information

Silver catalyst with high-energy surface prepared by plasma spraying for hydrogen evolution reaction

Yu-Yao Bai, Wen-Jing Kang, Cong Xi, Wen-Qi Yang, Zhe Li, Zi-Ang Ma, Cun-Ku Dong, Hui Liu, Jing Mao*,Fu-Xing Ye*, Xi-Wen Du*

Figures S1-S14

Table S1-S3

Experimental Section

Computational Methods and Models and relevant references

Table S1. Parameters of plasma spraying

| Instrument model	Plasma gas	Send powder gas	Arm walking speed	Spray distance	Voltage	current
APS-2000	Ar (6 atm)	N_2 (5 atm)	160 mm/s	160 mm	40 V	500 A

Table S2. Double layer capacitance and roughness factor of the samples

| Samples	Double layer capacitance (mF/cm^2)	Rough factor(RF)
PS-Ag	6.73	26.92
Ag powder	2.12	8.48
Ag foil	0.25	1

Table S3. Summary on HER properties of Ag-based electrocatalysts.

| Electrocatalysts	Electrolytes	j (mA cm^{-2})	Overpotential (mV)	Ref.
PS-Ag	0.5 M H_2SO_4	10	349	This work
Ag10/PPy	0.5 M H_2SO_4	10	459	1
Ag/Au-HPNSs@PFP-A	0.5 M H_2SO_4	10	400	2
Ag_2Se	0.5 M H_2SO_4	10	367	3
Ag/Ag_2S	0.5 M H_2SO_4	10	370	4
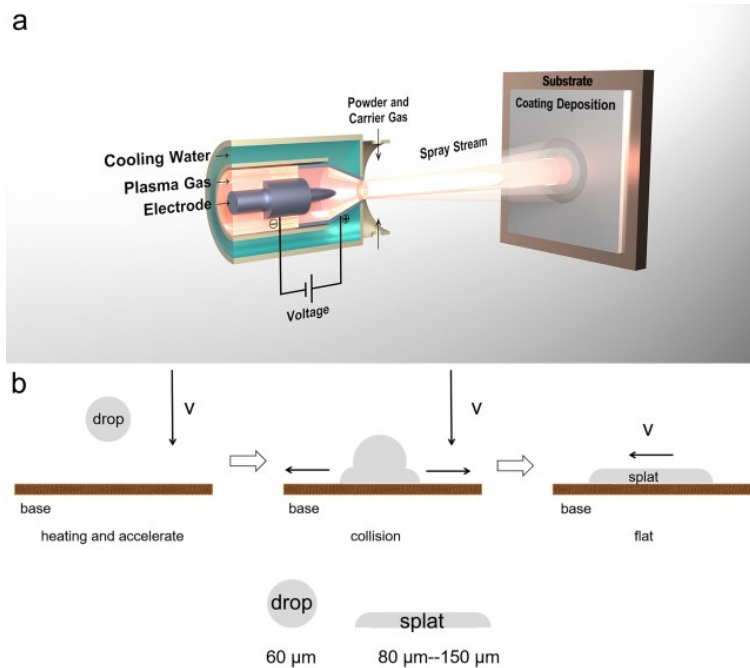
Fig. S1. (a) Schematic diagram of plasma spraying process. (b) Schematic diagram of the formation of spraying coating.
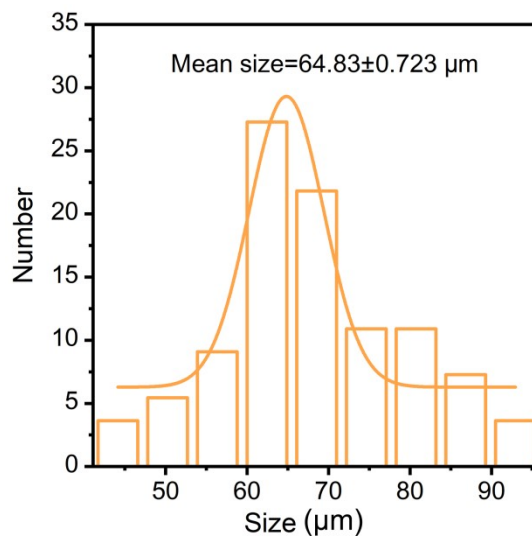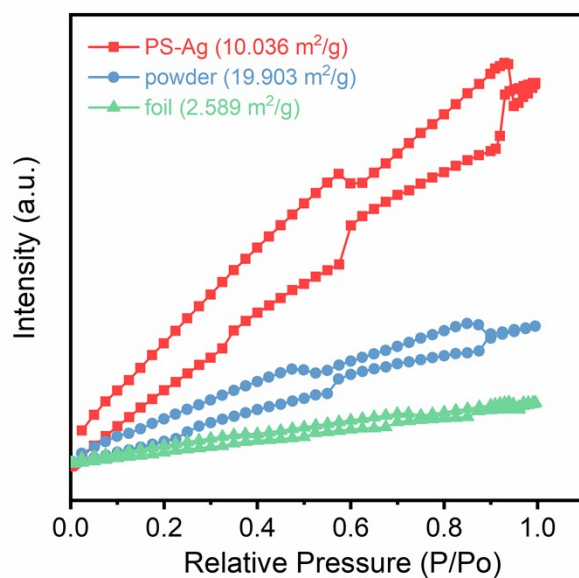

**Fig. S2.** Size distribution of silver particles in raw powder.
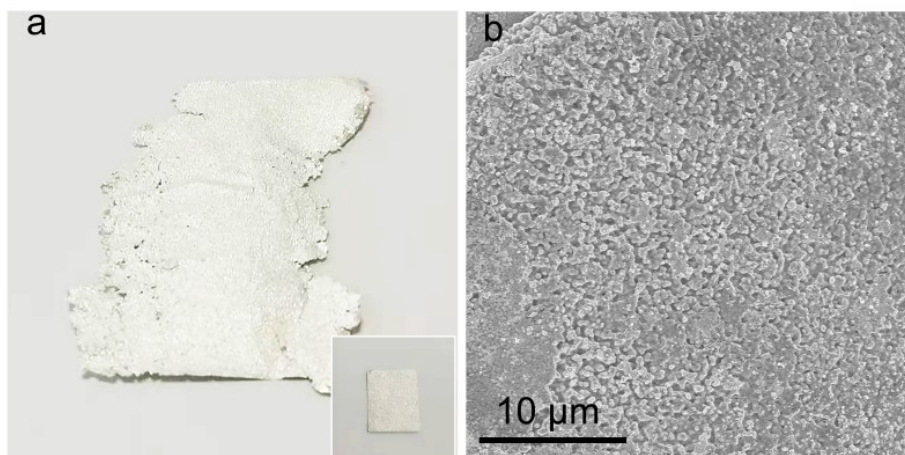
Fig. S3. (a) Optical image of the free-standing silver coating layer formed by plasma spraying, the inset shows the self-supporting electrode which was cut from the coating with size of 1×0.5 cm^2.   (b) High magnification SEM image of silver coating layer.

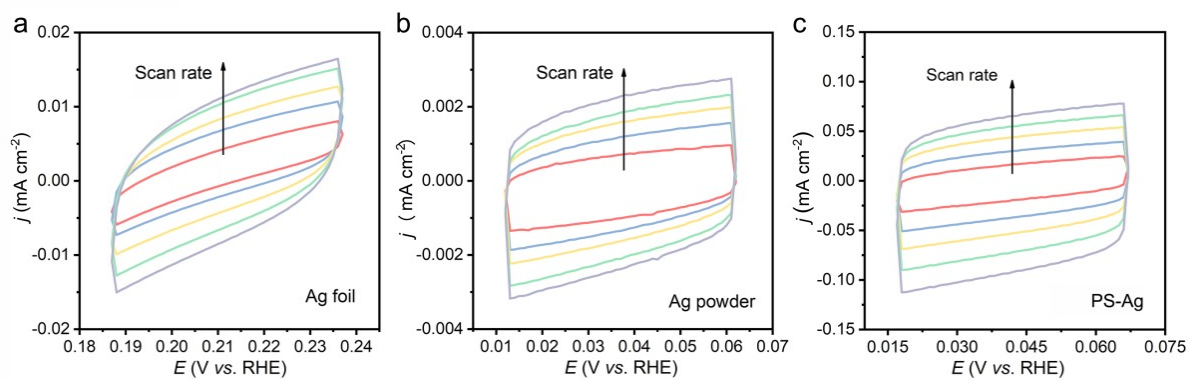**Fig. S4.** Physical specific surface area of PS-Ag, silver foil and silver powder.
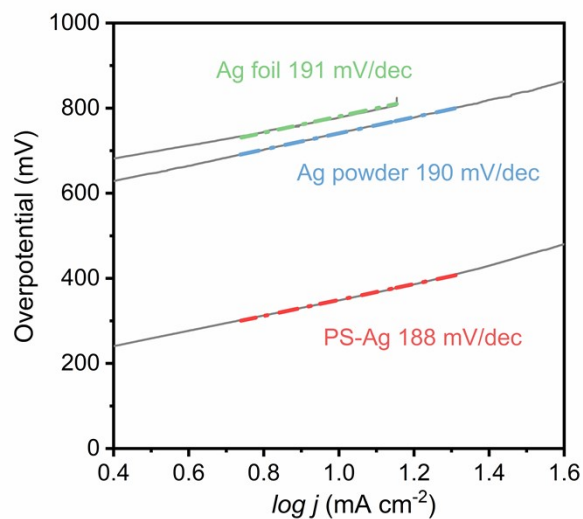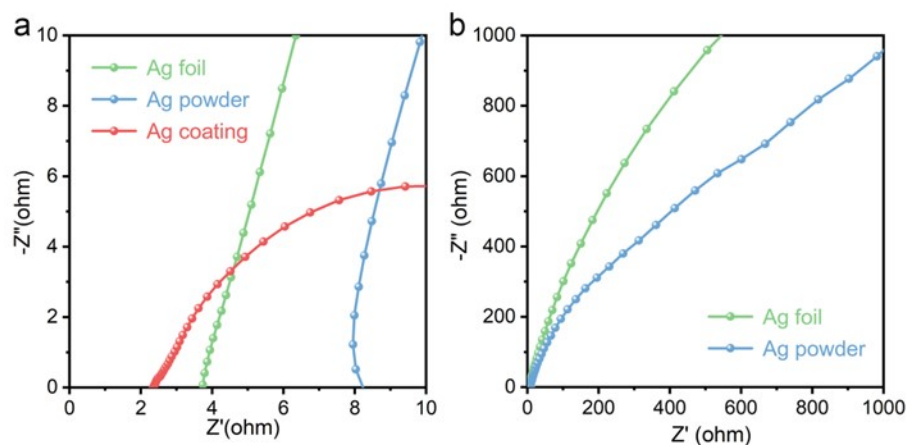
Fig. S5. Tafel slopes of PS-Ag, Ag powder and Ag foil

Fig. S6. CV curves at different scan rates. (a) Ag foil, (b) Ag powder, (c) PS-Ag.

Fig. S7. (a)The starting position of EIS curve of silver coating, silver powder and silver foil. (b)The overall trend of EIS curve of silver powder and foil.
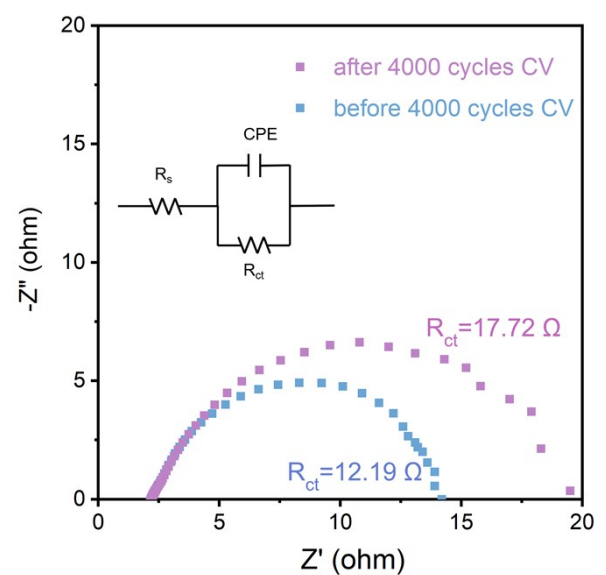
Fig. S8. Nyquist plots of PS-Ag before and after 4000 cycles CV test.
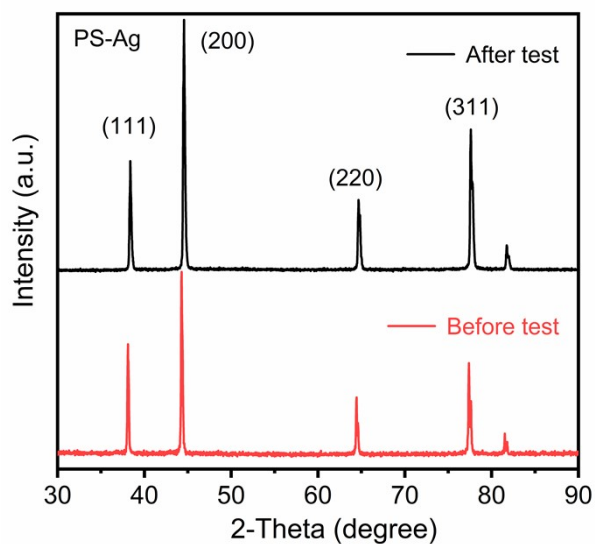
Fig. S9. XRD of PS-Ag before and after electrochemical testing.

Fig. S10. XPS spectrum of PS-Ag before and after electrochemical testing.

Fig. S11 The relative intensity of XRD peaks with different crystal surfaces.

Fig. S12. High resolution TEM image of PS-Ag.

Fig. S13. Atomic models for DFT calculation.

SUPPORTING INFORMATION

Experimental Section

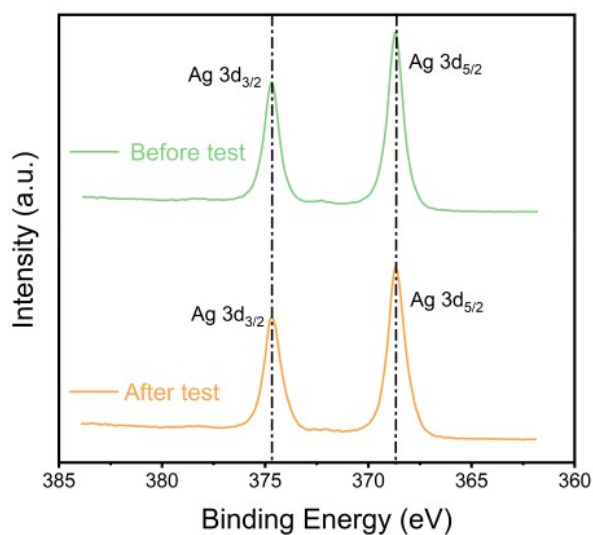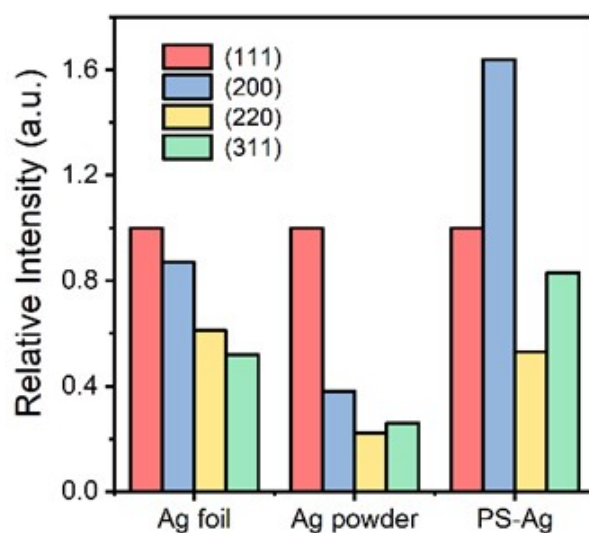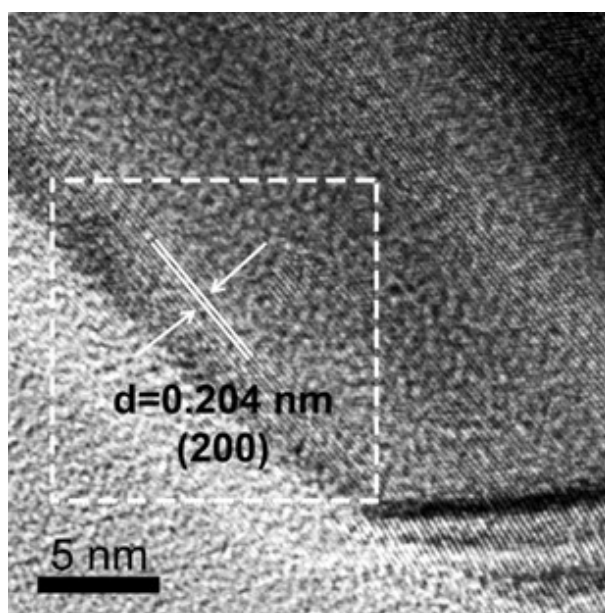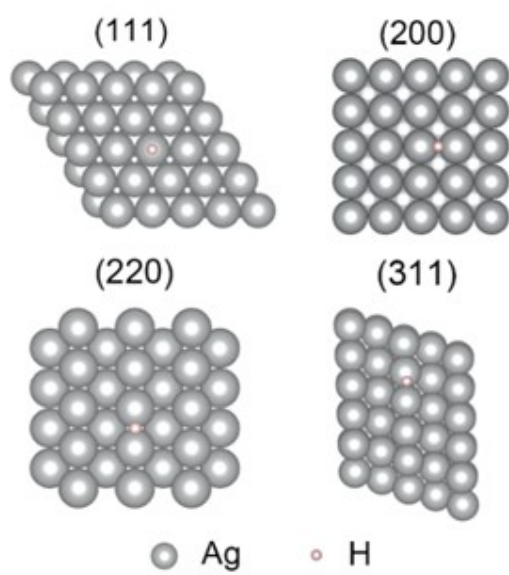**Preparation of Ag electrodes.** The plasma spraying was performed on a APS-2000 spraying machine, and the experimental parameters are shown in **Table S1**. The raw material is commercial silver powder with a diameter of about 64 μm.

Material Characterizations. The phase constitutions of samples were detected by X-ray diffraction (XRD, Bruker D8 Advance) with Cu Kα radiation source and Ni filter, and Cu tube with 1.5418 Å. The morphology was observed by scanning electron microscopy (SEM, Hitachi S-4800). Transmission electron microscopy (TEM) was performed by using a FEI Technai G2 F20 transmission electron microscope.Axis Supra X-ray photoelectron spectrometer (XPS) produced by Kratos Analytical Ltd., which uses aluminum Ka microfocusing monochromator as X-ray source for quantitative analysis of elemental valence states of samples. Nitrogen adsorption specific surface area analyzer (BET,asiQM0002-5) was used to test the specific surface area of the samples. It used a single-phase power supply of 220 V with a frequency of 50 Hz and a maximum power of 1100 VA.

Electrochemical Measurements. The acid HER performance was measured in in a quartz cell filled with N_2 saturated 0.5 M H_2SO_4. A standard three-electrode system was used in electrochemical tests, of which saturated calomel electrode (SCE) is the reference electrode, carbon rod is counter electrode and PS-Ag is the self-supported working electrode. The potential relative to SCE can be converted into that relative to reversible hydrogen electrode (RHE) according to the following formula:

$$E_{RHE}(V) = E_{SCE}(V) + 0.242V + 0.0592V \times pH_{electrolyte}$$

The electrochemical tests were performed on a workstation CHI601E at room temperature. To confirm the accuracy of the test results, self-supported Pt/C electrode was tested under the same conditions. All samples were scanned by cyclic voltammetry (CV) at 50 mV/s for 20 cycles to stabilize the sample and then tested for linear sweep voltammetry (LSV). During HER process, the catalyst remained in the metallic state and was not oxidized because the redox potential of silver (E_θ (Ag^+/Ag) =0.7996 V vs. RHE) was much higher than that of hydrogen (E_θ (H^+/H_2) = 0 V vs. RHE).

The electrochemically active surface area (ECSA) was obtained by measuring the double-layer capacitance (C_{dl}) in the non-Faraday region. The CV cycles were carried out in 0.5 M H_2SO_4 solution at sweep rates of 15 mV/s, 30 mV/s, 45 mV/s, 60 mV/s and 75 mV/s, respectively.

SUPPORTING INFORMATION

Computational Methods and Models. Spin-polarized density functional theory (DFT) calculations were performed using the Vienna ab initio Simulation Package (VASP)[5-8]. The revised Perdew-Burke-Ernzerhof (PBE)[9]exchange-correlation functional of the generalized gradient approximation (GGA) was used with the projector-augmented wave (PAW) pseudopotential[10]. A plane-wave cutoff energy of 500 eV was used for all geometry optimizations and the structure geometry was fully optimized until the residual force was less than 0.03 eV/Å without any constraints. Four-layer of 4x4 Ag with four common exposed facets (200) (220) (111) (311) were considered. For the calculation of adsorption energies, the bottom two layers of the metal were fixed to their optimized positions, while the upper two layers and adsorbates were fully relaxed. K points were sampled using a $5 \times 5 \times 1$ Monkhorst-Pack mesh to ensure an accurate energy value[10]. A vacuum layer of 15 Å thick was applied perpendicular to the slabs to avoid artificial interactions between the slab and its periodic images.

The binding energies (E_b) of an adsorbate on the surface is defined here as:

$$E_b \text{ (adsorbate)} = E_b \text{ (adsorbate + surface)} - E_b \text{ (surface)} - E_b \text{ (adsorbate)} \quad (1\text{-}1)$$

where E_b (adsorbate + surface), E_b (surface) and E_b (adsorbate) are the total energies of optimized adsorbate and surface, clean surface, and adsorbate in the gas phase, respectively. Therefore, a more negative binding energy value means the formation of derivative is thermodynamically more favorable.

References

1. M. Sabalová, R. Oriňaková, A. Oriňak, I. Smoradová, M. Kupková and M. Strečková, *Chem Pap*, 2017, **71**, 513-523.
2. Z. Zhao, H. Wu, C. Li, *Energy,* 2021, **218**, 119520.
3. S. Hussain, J. Chae, K. Akbar, D. Vikraman, L. Truong, B. A. Naqvi, Y. Abbas, H. Kim, S. Chun, G. Kim and J. Jung, *Nanomaterials-Basel*, 2019, **9**, 1460.
4. C. M. Cova, A. Zuliani, A. R. Puente Santiago, A. Caballero, M. J. Muñoz-Batista and R. Luque, *J Mater Chem A*, 2018, **6**, 21516-21523.
5. G. Kresse, J. Hafner, *Phys. Rev., B Condens. Matter*, 1993, **47**, 558-561.
6. G. Kresse, J. Hafner, *Phys. Rev., B Condens. Matter*, 1994, **49,** 14251-14269.
7. G. Kresse, J. Furthmüller, *Phys. Rev., B Condens. Matter*, 1996, **54**, 11169-11186.
8. G. Kresse, J. Furthmüller, *Comput. Mater. Sci.*, 1996, **6**, 15-50.
9. John P. Perdew, Kieron Burke, Matthias Ernzerhof, *Phys. Rev. Lett.*, 1996,**77**, 3865.

10. Hendrik J. Monkhorst, James D. Pack, *Phys. Rev., B Condens. Matter*, 1976, **13**, 5188-5192.